HAL
open science

Giant shot noise from Majorana zero modes in topological trijunctions

T. Jonckheere, J. Rech, A. Zazunov, R. Egger, A. Levy Yeyati, T. Martin

To cite this version:

T. Jonckheere, J. Rech, A. Zazunov, R. Egger, A. Levy Yeyati, et al.. Giant shot noise from Majorana zero modes in topological trijunctions. Physical Review Letters, 2019, 122 (9), pp.097003. 10.1103/PhysRevLett.122.097003 . hal-01902947

HAL Id: hal-01902947

https://hal.science/hal-01902947v1

Submitted on 25 Mar 2019

HAL is a multi-disciplinary open access archive for the deposit and dissemination of scientific research documents, whether they are published or not. The documents may come from teaching and research institutions in France or abroad, or from public or private research centers.

L'archive ouverte pluridisciplinaire **HAL**, est destinée au dépôt et à la diffusion de documents scientifiques de niveau recherche, publiés ou non, émanant des établissements d'enseignement et de recherche français ou étrangers, des laboratoires publics ou privés.

arXiv:1809.10527v2 [cond-mat.supr-con] 20 Feb 2019

Giant shot noise from Majorana zero modes in topological trijunctions

T. Jonckheere,[1] J. Rech,[1] A. Zazunov,[2] R. Egger,[2] A. Levy Yeyati,[3] and T. Martin[1]
[1] *Aix Marseille Univ, Université de Toulon, CNRS, CPT, Marseille, France*
[2] *Institut für Theoretische Physik, Heinrich Heine Universität, D-40225 Düsseldorf, Germany*
[3] *Departamento de Física Teórica de la Materia Condensada C-V, Condensed Matter Physics Center (IFIMAC) and Instituto Nicolás Cabrera, Universidad Autónoma de Madrid, E-28049 Madrid, Spain*
(Dated: February 21, 2019)

The clear-cut experimental identification of Majorana bound states in transport measurements still poses experimental challenges. We here show that the zero-energy Majorana state formed at a junction of three topological superconductor wires is directly responsible for giant shot noise amplitudes, in particular at low voltages and for small contact transparency. The only intrinsic noise limitation comes from the current-induced dephasing rate due to multiple Andreev reflection processes.

Introduction.—Majorana fermions have emerged as quasi-particles of central importance in modern condensed matter physics, e.g., for topological superconductors (TSs) and in exotic phases with intrinsic topological order [1–7]. In one-dimensional TS wires, spatially localized Majorana bound states (MBSs) are formed at the wire boundaries. The corresponding Majorana operator represents a quasi-particle that equals its own antiparticle. MBSs are associated with non-Abelian braiding statistics, and a pair of well-separated MBSs defines a non-local zero-energy fermion state. Apart from the obvious fundamental interest, stable and robust realizations of zero-energy MBSs would also enable powerful topologically protected quantum information processing schemes [1, 5, 8–11]. Over the past few years, many experiments have reported evidence for MBSs either through the observation of conductance peaks in transport spectroscopy (with normal probe leads tunnel-coupled to MBSs) [12–21] or from signatures of the 4π periodic Josephson current-phase relation in TS-TS junctions [22–25]. However, in principle both types of experiments are not able to firmly rule out alternative physical mechanisms. In fact, zero-bias anomalies are ubiquitous and could arise from many sources, e.g., subgap Andreev states [26, 27] or disorder [28, 29]. Moreover, various types of topologically trivial Josephson junctions can also produce 4π periodic current-phase relations [30–33].

Fortunately, by investigating only slightly more elaborate devices, experiments could be in a position to detect very clear MBS signals that are much harder to fake. For instance, in mesoscopic TS devices characterized by a strong Coulomb charging energy, highly nonlocal conductance phenomena are predicted for very low temperatures in the presence of zero-energy MBSs [34–37]. On the other hand, transport in a three-terminal device composed of a TS wire and two normal wires should yield characteristic MBS features in the current-current cross correlations between the normal wires [38–44]: While shot noise in two-terminal setups also carries interesting information [45–50], in the three-terminal case already its sign has an unconventional voltage dependence given by $-\mathrm{sgn}(V_1V_2)$, where voltages V_1 and V_2 are applied between the TS and the respective normal wire [38–42]. A different — and even more distinct — Majorana manifestation in shot noise properties of topological trijunctions is described below.

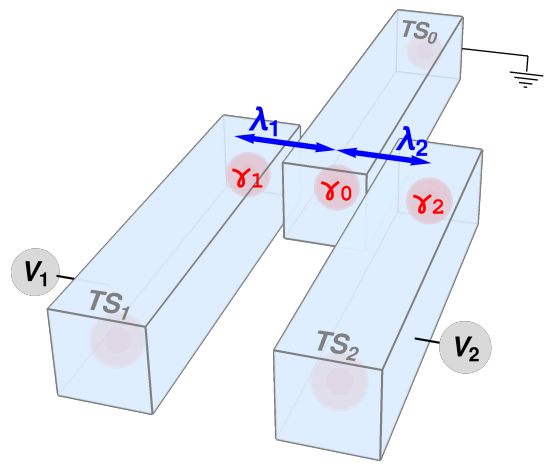

FIG. 1. Junction of three TS wires. The central wire (TS_0) with Majorana operator γ_0 is tunnel-coupled with amplitude λ_1 (λ_2) to the left, TS_1 (right, TS_2) wire with corresponding Majorana operator γ_1 (γ_2). A voltage V_1 (V_2) is applied between TS_1 (TS_2) and TS_0. MBSs at the far ends are also indicated.

We here point out that an experimentally identifiable and quite dramatic consequence of zero-energy MBSs arises when probing shot noise in a trijunction of three TS wires, see Fig. 1 for a schematic sketch. In this setup, an unpaired zero-energy MBS must exist on general grounds [9]. We show below that this MBS is directly responsible for giant shot noise levels. We here define the shot noise amplitude from the current-current correlations measured in the left or right (TS_1, TS_2) wires in Fig. 1, which are biased at voltages V_1 and V_2 against the central (TS_0) wire, respectively. The precise values of V_1 and V_2 are not crucial, and giant noise levels are found at least for all commensurate cases, $pV_1 = qV_2$ with inte-

ger p, q [55]. (The case of non-commensurate voltages is more complex and cannot be accessed with the methods used below.) We provide an intuitive explanation for the mechanism behind the giant noise levels by studying the atomic limit, where the TS gap Δ represents the largest energy scale. Calculations then simplify substantially and allow for an analytical understanding. By including above-gap continuum quasi-particles, we next show that the shot noise amplitude is limited by a current-induced dephasing rate due to multiple Andreev reflection (MAR) processes. The noise features are most pronounced at low voltage and small contact transparency, where the sub-gap current, and hence also the dephasing rate, is small. While the current shows similar MAR features as in TS-TS junctions [51–53], our results suggest that shot noise experiments for the setup in Fig. 1 should readily find clear MBS signatures.

Model.—The system is modeled by a generic low-energy Hamiltonian, $H = \sum_{\nu=0,1,2} H_{\mathrm{TS}_\nu} + H_t$, where each TS wire corresponds to (we often put $e = \hbar = v_F = 1$) [2]

$$H_{\mathrm{TS}_\nu} = \int_0^\infty dx\, \Psi_\nu^\dagger(x)\left(-i\partial_x\sigma_z + \Delta\sigma_y\right)\Psi_\nu(x), \qquad (1)$$

with Nambu spinors $\Psi_\nu = (c_{R,\nu}, c_{L,\nu}^\dagger)^T$ and assuming chemical potential $\mu = 0$. Here $c_{L/R,\nu}$ are left/right-moving, effectively spinless fermion operators in the TS_ν wire, and Pauli matrices $\sigma_{x,y,z}$ (identity σ_0) act in Nambu space. For notational simplicity, the gap Δ is assumed real and identical for all wires. The boundaries of the three wires at $x = 0$ are connected by the tunneling Hamiltonian H_t. With applied voltages $V_{j=1,2}$, gauge-invariant phase differences are given by $\varphi_j(t) = 2V_j t + \varphi_j(0)$. We put $\varphi_j(0) = 0$ but constant phase offsets could take into account, e.g., initial conditions or tunneling phase shifts. We choose a gauge where the $\varphi_j(t)$ appear only in H_t [42, 51],

$$H_t = \sum_{j=1,2} \lambda_j \left(e^{i\varphi_j(t)/2} c_j^\dagger c_0 + \mathrm{h.c.}\right), \qquad (2)$$

with $c_\nu = [c_{L,\nu} + c_{R,\nu}](x = 0)$. In our units, λ_j are dimensionless real tunneling amplitudes,

$$\lambda_1 = \lambda\cos\chi, \quad \lambda_2 = \lambda\sin\chi, \quad 0 \le \lambda \le 1, \qquad (3)$$

and the normal-state total transmission probability ('transparency') between TS_0 and TS_1, TS_2 is [42]

$$\tau = \frac{4\lambda^2}{(1+\lambda^2)^2}. \qquad (4)$$

Keldysh approach.—We solve this problem by using the Keldysh boundary Green's function (bGF) formalism [42, 51]. The Keldysh bGF of the uncoupled TS_ν wire is given by $\check{g}_\nu(t-t') = -i\left\langle \mathcal{T}_C \Psi_\nu(t)\Psi_\nu^\dagger(t')\right\rangle$, with the boundary Nambu spinor $\Psi_\nu = (c_\nu, c_\nu^\dagger)^T$ and the Keldysh time ordering operator $\mathcal{T}_C$. Retarded/advanced components of $\check{g}_\nu$ follow in frequency representation as [51]

$$g_\nu^{R/A}(\omega) = \frac{\sqrt{\Delta^2 - (\omega \pm i0^+)^2}\,\sigma_0 + \Delta\sigma_x}{\omega \pm i0^+}. \qquad (5)$$

The $\omega = 0$ pole in Eq. (5) describes the zero-energy MBS. Continuum quasi-particles appear at $|\omega| > \Delta$, with boundary density of states $\sim \sqrt{\omega^2 - \Delta^2}/|\omega|$ [51]. Physical quantities are expressed in terms of the full Keldysh bGF, $\check{G}$, which in turn follows by solving the Dyson equation, $\check{G} = (\check{g}^{-1} - \check{W})^{-1}$, where $\check{g} = \mathrm{diag}_L(\check{g}_0, \check{g}_1, \check{g}_2)$ is diagonal in lead space. The tunneling matrix, $\check{W} = \mathrm{diag}_K(W, -W)$, is diagonal in Keldysh space, where Eq. (2) yields the nonvanishing entries

$$W_{0,j=1,2}(t) = \lambda_j\sigma_z e^{i\sigma_z\varphi_j(t)/2}, \quad W_{j,0}(t) = W_{0,j}^\dagger(t). \qquad (6)$$

The time-dependent current flowing through TS_j, oriented toward the junction, corresponds to the Heisenberg operator

$$\hat{I}_j(t) = 2\frac{\partial H(t)}{\partial\varphi_j(t)} = i\Psi_j^\dagger(t)\sigma_z W_{j,0}(t)\Psi_0(t). \qquad (7)$$

With the average current $I_j(t) = \langle \hat{I}_j(t)\rangle$, current-current correlations for the $\mathrm{TS}_{j=1,2}$ wires are defined as

$$S_{jj'}(t,t') = \left\langle \hat{I}_j(t)\hat{I}_{j'}(t')\right\rangle - I_j(t)I_{j'}(t'). \qquad (8)$$

Below we discuss the zero-frequency noise, $S_{jj'} \equiv S_{jj'}(\omega = 0)$. For clarity, we focus on the case $V_1 = -V_2 = V$ from now on (but see [55]). However, the atomic limit results below are identical for $V_1 = V_2 = V$.

Numerical results.—After a double Fourier transform along with a summation over discrete frequency domains of width V, the Dyson equation reduces to a matrix inversion problem which we have solved numerically, cf. Ref. [54]. Given the solution for $\check{G}$, we directly obtain

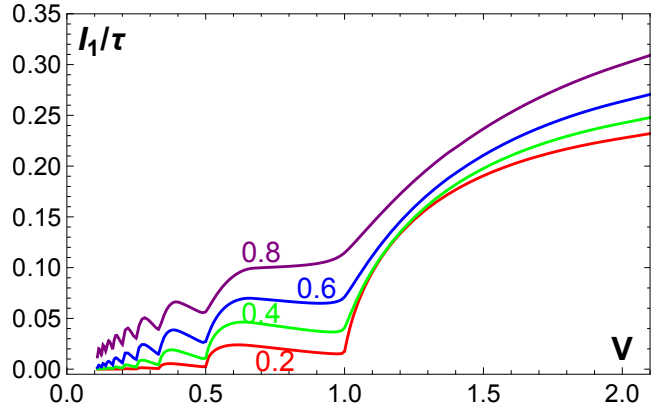

FIG. 2. Numerical results for the current I_1 (in units of $e\Delta/h$) vs voltage V (in Δ/e) for different transparencies τ, see Eq. (4), in a symmetric junction ($\lambda_1 = \lambda_2$) with $V_1 = -V_2 = V$. For better visibility, I_1 is divided by τ.

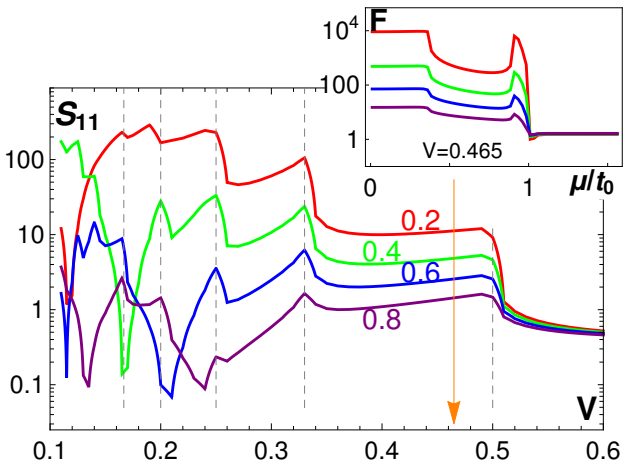

FIG. 3. Numerical results for shot noise S_{11} (in units of $e^2\Delta/h$) vs voltage V (in Δ/e) for different transparencies τ in a symmetric trijunction, cf. Fig. 2. Dashed vertical lines mark MAR onsets, $V = e\Delta/n$ with $n = 2, 3, \ldots, 6$. Inset: Fano factor F (on logarithmic scale) vs chemical potential μ/t_0 of TS_2, for $V = 0.465$ and bandwidth $t_0 = 10\Delta$.

the current-voltage characteristics as well as the zero-frequency shot noise amplitude. Figure 2 shows numerical results for the current-voltage characteristics, with qualitatively similar features as for TS-TS junctions [51–53]. In particular, MAR onsets are visible at $V = \Delta/n$ (integer n), and for low transparency and small V, the current becomes very small. Figure 3 illustrates our numerical shot noise results for $S_{11}(V)$. In contrast with the current, shot noise behaves in a totally different manner as compared to TS-TS junctions [6, 53]. Taking note of the logarithmic noise scale in Fig. 3, we observe giant noise levels which are particularly pronounced near MAR onsets. Remarkably, in contrast to the average current, the noise amplitude shows an overall *increase* when reducing the transparency τ. The inset of Fig. 3 demonstrates that these features are directly related to MBSs: The Fano factor, $F = S_{11}/(2eI_1)$, becomes small when one lead (here TS_2) exits the topological regime $|\mu|/t_0 < 1$ upon changing its chemical potential μ (with $\mu = 0$ in the other wires). Using the bGFs in Ref. [42], we find very large F for all $|\mu|/t_0 < 1$ (especially at small τ), with an abrupt drop down to $F \simeq 1$ for $|\mu|/t_0 > 1$. We next show analytically that the giant noise levels are tied to the existence of an unpaired zero-energy MBS.

Atomic limit.—Since the features in Fig. 3 are most pronounced for small V and low transparency, we consider the atomic limit where Δ represents the largest energy scale and the bGF (5) simplifies to

$$g_\nu^{R/A}(\omega) = \frac{\Delta}{\omega \pm i\eta}\begin{pmatrix} 1 & 1 \\ 1 & 1 \end{pmatrix}. \tag{9}$$

The small parameter $\eta > 0$ represents a finite parity relaxation rate (see below). By construction, the simplified bGF (9) neglects above-gap continuum states. Boundary fermions are thus projected to the Majorana sector, $c_\nu \to \sqrt{\Delta}\,\gamma_\nu$, where Majorana operators, $\gamma_\nu = \gamma_\nu^\dagger$, satisfy the anticommutation relations $\{\gamma_\nu, \gamma_{\nu'}\} = \delta_{\nu\nu'}$. The atomic limit Hamiltonian for an arbitrary trijunction thereby follows from the full $H(t)$ as, see Eq. (3),

$$\begin{aligned} H_{\mathrm{at}}(t) &= 2i\Omega(t)\left[\cos(\chi)\gamma_1 - \sin(\chi)\gamma_2\right]\gamma_0, \\ \Omega(t) &= \lambda\Delta\sin(Vt)\,. \end{aligned} \tag{10}$$

By passing to a rotated Majorana basis,

$$\begin{aligned} \gamma_- &= \cos(\chi)\gamma_1 - \sin(\chi)\gamma_2, \\ \gamma_+ &= \sin(\chi)\gamma_1 + \cos(\chi)\gamma_2, \end{aligned} \tag{11}$$

and combining γ_- and γ_0 to a complex fermion, $d = (\gamma_- + i\gamma_0)/\sqrt{2}$, one can solve the problem in an elementary manner. Indeed, $i\gamma_-\gamma_0 = d^\dagger d - 1/2$ is the only combination of Majorana operators appearing in H_{at}, and Eq. (10) thus affords the alternative representation

$$H_{\mathrm{at}}(t) = 2i\Omega(t)\gamma_-\gamma_0 = \Omega(t)(2d^\dagger d - 1), \tag{12}$$

where the parity $(-1)^{d^\dagger d}$ is always conserved. The Majorana operator γ_+, on the other hand, does not show up in the Hamiltonian and represents the zero-energy MBS of the trijunction. Expressing $\gamma_+ = (f + f^\dagger)/\sqrt{2}$ in terms of a zero-energy fermion f, the current operator (7) takes the form (say, for TS_1)

$$\begin{aligned} \hat{I}_1(t) &= 2i\lambda_1\Delta\cos(Vt)\left[\cos(\chi)\gamma_- + \sin(\chi)\gamma_+\right]\gamma_0 \\ &= \lambda_1\Delta\cos(Vt)\Big[\cos\chi\ (2d^\dagger d - 1) \\ &\qquad + \sin\chi\ (f + f^\dagger)(d - d^\dagger)\Big]. \end{aligned} \tag{13}$$

The non-trivial coupling between the d fermion and the zero-mode fermion f in Eq. (13) is ultimately responsible for giant noise levels. Although f does not appear in the Hamiltonian, it affects the current operator when all three TS wires are coupled together.

In (d, f) fermion representation, physical steady state density matrices must commute with H_{at} and therefore have the form $\rho_{\mathrm{s}} = \sum_{n,m=0,1} w_{nm}|nm\rangle\langle nm|$, where $w_{nm} \geq 0$ with $\sum_{nm} w_{nm} = 1$ is the statistical weight of the state $|nm\rangle = (d^\dagger)^n(f^\dagger)^m|0\rangle$. For a symmetric trijunction, we then obtain the average current in the atomic limit as

$$I_1^{(\mathrm{at})}(t) = \lambda\Delta\cos(Vt)(\langle d^\dagger d\rangle - 1/2). \tag{14}$$

As for a TS-TS junction [6], only the AC current with frequency $\omega = V$ can be finite. For the shot noise, with Eq. (13) and the Bessel J_1 function, we find [55]

$$S_{11}^{(\mathrm{at})} = \frac{\lambda^2\Delta^2}{4\eta}J_1^2\left(2\lambda\Delta/V\right), \tag{15}$$

which is limited only by the parity relaxation time $1/\eta$. Examples for Eq. (15) are shown in Fig. 4 and, for small V, agree rather well with the full numerics. For larger

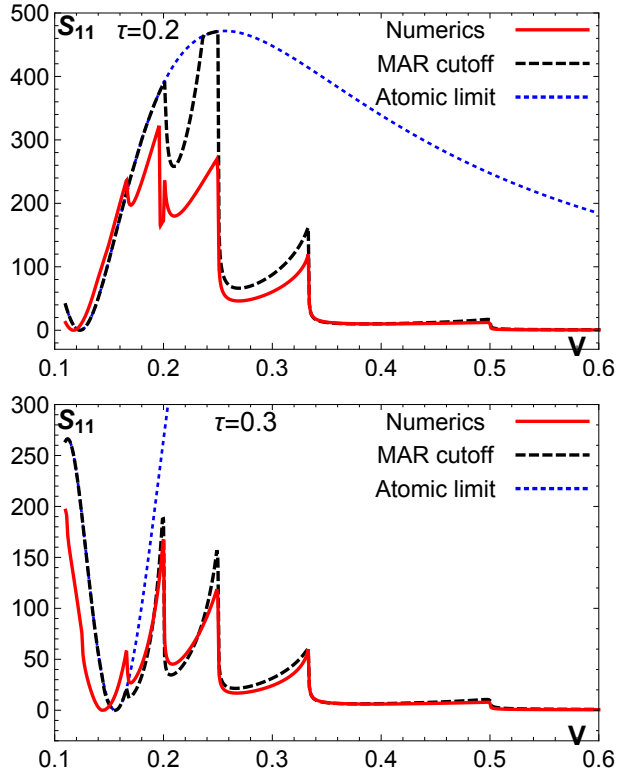

FIG. 4. Shot noise S_{11} vs voltage V for $\tau = 0.2$ (top) and $\tau = 0.3$ (bottom) in a symmetric trijunction. The atomic limit prediction (15) is shown for $\eta = 10^{-5}\Delta$ as blue dotted curve, full numerical results as solid red curves. Black dashed curves include MAR effects, see Eqs. (15) and (18).

V, the complex peak structure in $S_{11}(V)$ is missed by Eq. (15) and the noise level is overestimated. Figure 4 also shows a marked noise minimum at low voltage which shifts to smaller V as τ decreases. The position of the minimum corresponds to the first zero of the Bessel function in Eq. (15). Similar noise dips are also observable in the full numerical results in Fig. 3.

Discussion.—The giant noise features are deeply related to the existence of the zero mode γ_+, which also implies that the current operator and the Hamiltonian do not commute. One can understand the giant noise as a generic feature of periodically driven two-level systems. To that end, we note that three Majorana operators, $\gamma_{0,1,2}$, can equivalently be represented in terms of Pauli matrices. Choosing

$$\tau_z = 2i\gamma_1\gamma_0, \quad \tau_x = 2i\gamma_0\gamma_2, \tag{16}$$

we obtain the current operator, Eq. (13), in diagonal form, $\hat{I}_1(t) = \lambda_1\Delta\cos(Vt)\tau_z$. However, in this basis, $H_{\rm at}(t) = \Omega(t)[\cos(\chi)\tau_z + \sin(\chi)\tau_x]$ is not diagonal anymore. Since the τ_x part in $H_{\rm at}$ coherently rotates τ_z and hence $\hat{I}_1(t)$, we directly encounter a coherent current switch which has divergent shot noise in the absence of relaxation channels. Moreover, since a zero-energy MBS always exists in a TS trijunction [9], the giant noise features are robust when adding a finite hybridization between γ_1 and γ_2.

A complementary viewpoint follows by noting that the uncoupled system has three MBSs at the junction, where γ_0 resides at energy $E = 0$ while γ_1 (γ_2) correspond to $E = V$ ($E = -V$). Including the tunnel couplings, a resonant process similar to crossed Andreev reflection (CAR) exists where two electrons are emitted from TS_0. One of them enters TS_1 through γ_1, the other TS_2 via γ_2. In a sequential tunneling picture, the rate for this process is

$$\Gamma = \lambda^2\Delta^2 \int dE \left(\frac{\eta}{(E-V)^2+\eta^2}\right)^2 \frac{\lambda^2\Delta^2}{E^2+\eta^2}. \tag{17}$$

The first factor in the integrand comes from the density of states for the MBSs γ_1 and γ_2, while the second is due to the probability for a CAR process. To leading order in $1/\eta$, Eq. (17) yields $\Gamma = \lambda^4\Delta^4/(4\eta V^2)$. The sequential tunneling result for S_{11} then coincides with Eq. (15) to lowest order in $\lambda\Delta/V$ [55]. We remark that in fully transparent S-S junctions, thermal noise exhibits a similar phenomenon [56, 57]. Since MBSs are equal-probability superpositions of electrons and holes, the corresponding hole process also exists. We thus encounter no average DC current yet have giant shot noise.

MAR effects.—Finally, we take into account continuum states [55]. To that end, we split the boundary fermion as $c_\nu = \sqrt{\Delta}\gamma_\nu + a_\nu$, with the Majorana part as before but now supplemented by above-gap fermions (a_ν). H_t then includes (i) MBS-MBS couplings as in Eq. (10), (ii) MBS-continuum couplings, and (iii) continuum-continuum terms. The latter terms are irrelevant for $V \ll \Delta$ and low transparency, while type (ii) terms, which correspond to MAR processes, can change the parity $(-1)^{d^\dagger d}$. This implies a loss of coherence for the d fermion dynamics. The average time between two tunneling processes of type (ii) defines a long-time cutoff, $T_{\rm MAR}$, limiting the integration of current correlations. A good approximation is given by $T_{\rm MAR}(V) = N_1/I_1(V)$, where $N_1 = 1 + \lfloor \Delta/V \rfloor$ is the number of electrons transferred in one MAR process. The dominant MAR effects on shot noise can then be taken into account by replacing η in Eq. (15) by a voltage-dependent effective parity relaxation rate,

$$\eta \to \eta_{\rm eff}(V) = \max\left(T_{\rm MAR}^{-1}(V), \eta\right), \tag{18}$$

where η is here due to additional parity relaxation channels and 'parity' refers to the Majorana sector only. Results obtained from Eq. (18) are shown in Fig. 4 and exhibit quantitative agreement with our full numerics. In particular, the peak pattern is now correctly reproduced without fitting parameter. The agreement is not quantitative when $T_{\rm MAR} \approx 1/\eta$, where Eq. (18) is too simplistic, cf. the case $\tau = 0.2$ in Fig. 4.

Conclusions.—The topological trijunction in Fig. 1 provides an attractive setup for experimental studies: an

unpaired zero-energy MBS is directly responsible for giant shot noise. Moreover, by measuring the detailed voltage dependence of the shot noise, precious information on parity relaxation rates can be obtained. If the MBSs are tunnel-coupled to additional low-energy states, e.g., because of finite wire length or due to fermion states localized near the junction, we expect a partial suppression of the shot noise amplitudes [55]. However, extrinsic noise sources are at odds with the predicted MAR features and can easily be ruled out. Finally, let us note that similar giant shot noise might be obtained in systems containing more than 3 TS electrodes - in particular for an odd number of TS (e.g. 5) one expects that a zero-mode should always be present. However the strong robustness with respect to the parameters might be specific to the 3TS case, which is also the most accessible experimentally.

ACKNOWLEDGMENTS

This work has been supported by the Excellence Initiative of Aix-Marseille University – A∗MIDEX, a French 'investissements d'avenir' program, by the Deutsche Forschungsgemeinschaft within Grants No. EG 96/11-1 and CRC TR 183 (project C04), by the Spanish MINECO through Grant Nos. FIS2014-55486-P and FIS2017-84860-R, and through the 'María de Maeztu' Program (MDM-2014-0377).

Appendix A: Shot noise in the atomic limit

In this section, we outline the calculation of the zero-frequency noise in the TS_1 lead, which is given by

$$S_{11} = \frac{1}{T_V}\int_0^{T_V} dt_+ \int_{-\infty}^{\infty} dt_- S_{11}\left(t_+ + \frac{t_-}{2}, t_+ - \frac{t_-}{2}\right), \tag{A1}$$

where $T_V = 2\pi/V$. The current-current correlator $S_{11}(t,t')$ is defined by Eq. (8) in the main text. In the atomic limit, one has [cf. Eqs. (10)-(14) in the main text]

$$S_{11}^{(\mathrm{at})}(t,t') = \mathrm{tr}\left\{\rho_\mathrm{s}\hat{\mathcal{I}}_1(t)\hat{\mathcal{I}}_1(t')\right\} - I_1^{(\mathrm{at})}(t)I_1^{(\mathrm{at})}(t'), \tag{A2}$$

where $\hat{\mathcal{I}}_1(t) = \mathcal{U}^\dagger(t,0)\hat{I}_1(t)\mathcal{U}(t,0)$, $\mathcal{U}(t,0) = \mathcal{T}\exp\{-i\int_0^t d\tau H_\mathrm{at}(\tau)\}$ is the time-evolution operator, $\mathcal{T}$ is the time-ordering operator, and the (steady state) density matrix ρ_s has been introduced in the main text. For a symmetric junction, $\lambda_1 = \lambda_2 = \lambda/\sqrt{2}$, one obtains

$$S_{11}^{(\mathrm{at})}(t,t') = \lambda^2\Delta^2\cos(Vt)\cos(Vt') \times \left[\mathrm{tr}\left\{\rho_\mathrm{s}X(t)X(t')\right\} - \left(n_d - \frac{1}{2}\right)^2\right], \tag{A3}$$

where $n_d = \mathrm{tr}\left\{\rho_\mathrm{s}d^\dagger d\right\}$ and

$$X(t) = d^\dagger d - \frac{1}{2} + \frac{1}{2}\left(f + f^\dagger\right)\left(de^{-i\Phi(t)} - d^\dagger e^{i\Phi(t)}\right) \tag{A4}$$

with $\Phi(t) = (2\lambda\Delta/V)[1-\cos(Vt)]$. Taking the trace over the fermions (d,f) yields

$$S_{11}^{(\mathrm{at})}(t,t') = \lambda^2\Delta^2\cos(Vt)\cos(Vt')\left[n_d\left(1-n_d\right) + \frac{1}{4}\left\{\cos\Phi(t,t') + i\left(2n_d - 1\right)\sin\Phi(t,t')\right\}\right], \tag{A5}$$

where $\Phi(t,t') = \Phi(t) - \Phi(t')$. Substituting Eq. (A5) into Eq. (A1) and using the expansion [58]

$$e^{iz\cos\theta} = \sum_{k=-\infty}^{\infty} i^k J_k(z)e^{ik\theta}, \tag{A6}$$

where $J_k(z)$ is the Bessel function of order k, one arrives at a formally divergent expression for the zero-frequency noise,

$$S_{11}^{(\mathrm{at})} = \frac{\pi}{2}\delta(\omega=0)\lambda^2\Delta^2 J_1^2\left(2\lambda\Delta/V\right). \tag{A7}$$

Note that in contrast to the current $I_1^{(\mathrm{at})}(t)$, the noise $S_{11}^{(\mathrm{at})}$ does not depend on the state of the Majorana fermion subsystem. Equation (A7) is then regularized by introducing a finite parity relaxation rate η, cf. Eq. (9) in the main text, with $2\pi\delta(0) = \int dt_- \to 1/\eta$. Hence we obtain Eq. (15).

Using the asymptotic forms of $J_1(z)$ at small and large z, one gets, respectively,

$$S_{11}^{(\mathrm{at})} \sim \frac{\lambda^4\Delta^4}{4\eta V^2} \quad \text{for } \lambda\Delta \ll V, \tag{A8}$$

$$S_{11}^{(\mathrm{at})} \sim \frac{\lambda\Delta V}{4\pi\eta}\cos^2\left(\frac{2\lambda\Delta}{V} - \frac{3\pi}{4}\right) \quad \text{for } \lambda\Delta \gg V. \tag{A9}$$

The crossover from $1/V^2$ to linear in V behavior with decreasing V indicates that $S_{11}^{(\mathrm{at})}$ must vanish in the limit $V \to 0$ (not accessible numerically). At the same time, $S_{11}^{(\mathrm{at})}$ exhibits oscillations with $1/V$ at sufficiently low V.

Appendix B: Dissipative effects on Majorana-induced noise

At low voltage $|V| \ll \Delta$, MAR processes may trigger transitions between the adiabatic Andreev level (d-fermion) and continuum states above the gap. These processes cause random flips of the pseudospin $S_d = d^\dagger d - 1/2$, which eventually leads to a suppression of the supercurrent noise associated with the zero mode f.

Assuming that (i) the noise due to pseudospin fluctuations is dominating and that (ii) hybridization of the f-fermion with continuum states is very weak and can be neglected, one obtains

$$S_{11}(t,t') \approx \lambda^2\Delta^2\cos(Vt)\cos(Vt') \times \left[\langle\delta S_d(t)\delta S_d(t')\rangle + \frac{1}{4}\left\langle d^\dagger(t)d(t') + d(t)d^\dagger(t')\right\rangle\right], \tag{B1}$$

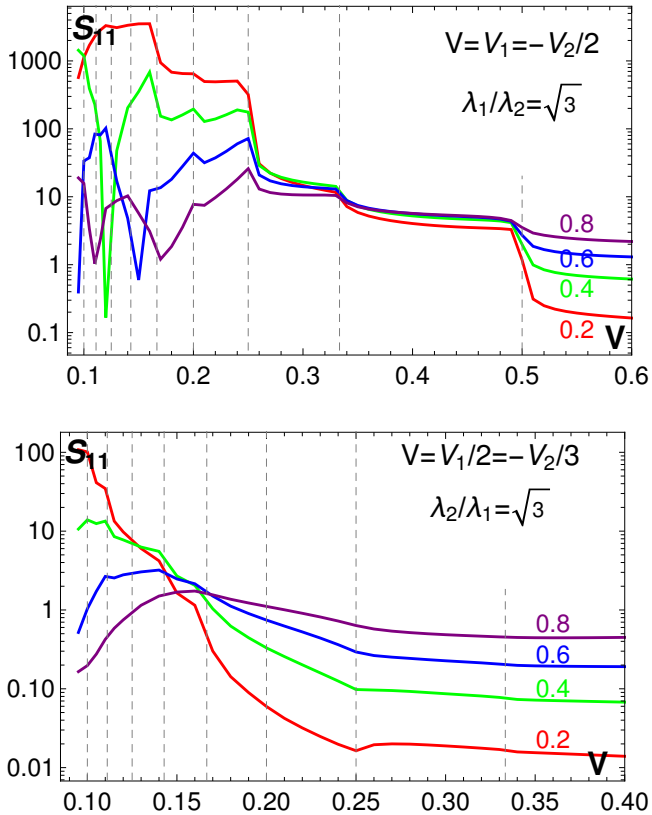

FIG. 5. Shot noise S_{11} (in units of $e^2\Delta/h$) vs voltage V (in Δ/e) for different transparencies from $\tau = 0.2$ to $\tau = 0.8$. We study two commensurate voltage configurations, $pV_1 = qV_2$. The top panel is for $p = 2$ and $q = -1$, with asymmetric tunnel couplings $\lambda_1/\lambda_2 = \sqrt{3}$. The bottom panel shows the case $p = 3$ and $q = -2$ for $\lambda_1/\lambda_2 = 1/\sqrt{3}$.

with $\delta S_d(t) = S_d(t) - \langle S_d(t)\rangle$. On long time scales, $|t - t'| \gg \omega_S^{-1}$, where ω_S is the frequency of pseudospin flips due to quasiparticle tunneling, one has $\langle \delta S_d(t)\delta S_d(t')\rangle \approx 0$, with $\langle S_d(t)\rangle = 0$. For short time scales, $|t - t'| \lesssim \omega_S^{-1}$, we still have

$$\left\langle d^\dagger(t)d(t') + d(t)d^\dagger(t')\right\rangle \approx \frac{1}{2}\, e^{i\Phi(t,t')} + \text{c.c.} \qquad \text{(B2)}$$

Applying again the identity (A6) and averaging over the 'center-of-mass' time t_+, cf. Eq. (A1), the zero-frequency shot noise takes the form

$$S_{11} = \frac{\lambda^2\Delta^2}{16}\int_{-\infty}^{\infty} d\tau \sum_{s,s'=\pm 1} i^{s+s'} \times \sum_{n=-\infty}^{\infty} J_{n+s}(Q/V)J_{n-s'}(Q/V)\cos(nV\tau), \qquad \text{(B3)}$$

with $Q = 2\lambda\Delta$. Here the nV harmonics are associated with the charge transfer ne due to MAR processes. Pseudospin flips are now readily incorporated by replacing $e^{inV\tau} \to e^{inV\tau - \Gamma_n|\tau|}$ in Eq. (B3), where the partial rates $\Gamma_{n\geq 1} = \Gamma_{-n}$ can be estimated similarly as in a two-terminal case, cf. Ref. [59], while $\Gamma_0 \sim \eta$ is the parity relaxation rate in the absence of MAR processes. As a result, we obtain

$$S_{11} = \frac{\lambda^2\Delta^2}{8}\sum_{n=-\infty}^{\infty}\frac{\Gamma_n}{n^2V^2 + \Gamma_n^2} \times \left[J_{n+1}(Q/V) - J_{n-1}(Q/V)\right]^2. \qquad \text{(B4)}$$

In particular, in the atomic limit one has $\Gamma_n = \Gamma_0\delta_{n0}$, and Eq. (B4) reduces to Eq. (15) in the main text.

Suppression of the giant noise can also arise from additional subgap states hybridized with the Majorana fermions γ_ν at the trijunction. For instance, this can be due to (i) exponentially small couplings between Majorana states located at opposite ends of finite-length TS wires and/or due to (ii) hybridization between γ_ν and low-energy impurity states localized near the contact region. At the phenomenological level, such 'quasiparticle poisoning' effects can be taken into account by introducing a corresponding parity relaxation rate, $\Gamma_{\rm qp}$, cf. Eq. (B1),

$$S_{11}(t,t') \approx \lambda^2\Delta^2\cos(Vt)\cos(Vt')\Big[\langle\delta S_d(t)\delta S_d(t')\rangle + \frac{1}{4}\left\langle d^\dagger(t)d(t') + d(t)d^\dagger(t')\right\rangle e^{-\Gamma_{\rm qp}|t-t'|}\Big]. \qquad \text{(B5)}$$

As a result, $\Gamma_{\rm qp}$ is added to the rates of MAR subharmonics, implying $\Gamma_n \to \Gamma_n + \Gamma_{\rm qp}$ in Eq. (B4).

Appendix C: Other configurations

We here demonstrate that giant noise appears in general for commensurate voltage configurations, $pV_1 = qV_2$ with integer p, q, where the case $pq = \pm 1$ has been studied in the main text. In Fig. 5, we show numerical results for two other examples, where we also allow for asymmetric tunnel couplings, $\lambda_1/\lambda_2 \neq 1$. The results in Fig. 5 illustrate that giant noise is generically observed for commensurate voltages. We note that for larger values of $|pq|$, somewhat lower V are required to reach comparably high noise levels. Finally, Fig. 5 also underlines the robustness of giant noise features against asymmetries in the tunnel couplings. In fact, this robustness already follows from our analytical calculations in the atomic limit, see Sec. A and the main text.

[1] C. Nayak, S.H. Simon, A. Stern, M. Freedman, and S. Das Sarma, Rev. Mod. Phys. **80**, 1083 (2008).
[2] J. Alicea, Rep. Prog. Phys. **75**, 076501 (2012).
[3] M. Leijnse and K. Flensberg, Semicond. Sci. Techn. **27**, 124003 (2012).

[4] C.W.J. Beenakker, Annu. Rev. Con. Mat. Phys. **4**, 113 (2013).
[5] S. Das Sarma, M. Freedman, and C. Nayak, npj Quantum Information **1**, 15001 (2015).
[6] R. Aguado, Rivista del Nuovo Cimento **40**, 523 (2017).
[7] R.M. Lutchyn, E.P.A.M. Bakkers, L.P. Kouwenhoven, P. Krogstrup, C.M. Marcus, and Y. Oreg, Nat. Rev. Mater. **3**, 52 (2018).
[8] A.Yu. Kitaev, Usp. Fiz. Nauk (Suppl) **171**, 131 (2001).
[9] J. Alicea, Y. Oreg, G. Refael, F. von Oppen, and M.P.A Fisher, Nature Phys. **7**, 412 (2011).
[10] S. Plugge, A. Rasmussen, R. Egger, and K. Flensberg, New J. Phys. **19**, 012001 (2017).
[11] T. Karzig, C. Knapp, R.M. Lutchyn, P. Bonderson, M.B. Hastings, C. Nayak, J. Alicea, K. Flensberg, S. Plugge, Y. Oreg, C.M. Marcus, and M.H. Freedman, Phys. Rev. B **95**, 235305 (2017).
[12] V. Mourik, K. Zuo, S.M. Frolov, S.R. Plissard, E.P.A. Bakkers, and L.P. Kouwenhoven, Science **336**, 1003 (2012).
[13] S. Nadj-Perge, I.K. Drozdov, J. Li, H. Chen, S. Jeon, J. Seo, A.H. MacDonald, B.A. Bernevig, and A. Yazdani, Science **346**, 602 (2014).
[14] M. Ruby, F. Pientka, Y. Peng, F. von Oppen, B.W. Heinrich, and K.J. Franke, Phys. Rev. Lett. **115**, 197204 (2015).
[15] S.M. Albrecht, A.P. Higginbotham, M. Madsen, F. Kuemmeth, T.S. Jespersen, J. Nygård, P. Krogstrup, and C.M. Marcus, Nature **531**, 206 (2016).
[16] M.T. Deng, S. Vaitiekenas, E.B. Hansen, J. Danon, M. Leijnse, K. Flensberg, J. Nygård, P. Krogstrup, and C.M. Marcus, Science **354**, 1557 (2016).
[17] F. Nichele, A.C.C. Drachmann, A.M. Whiticar, E.C.T. O'Farrell, H.J. Suominen, A. Fornieri, T. Wang, G.C. Gardner, C. Thomas, A.T. Hatke, P. Krogstrup, M.J. Manfra, K. Flensberg, and C.M. Marcus, Phys. Rev. Lett. **119**, 136803 (2017).
[18] H.J. Suominen, M. Kjaergaard, A.R. Hamilton, J. Shabani, C.J. Palmstrøm, C.M. Marcus, and F. Nichele, Phys. Rev. Lett. **119**, 176805 (2017).
[19] S. Gazibegovich, D. Car, H. Zhang, S.C. Balk, J.A. Logan, M.W.A. de Moor, M.C. Cassidy, R. Schmits, D. Xu, G. Wang, P. Krogstrup, R.L.M. Op het Veld, J. Shen, D. Bouman, B. Shojaei, D. Pennachio, J.S. Lee, P.J. van Veldhoven, S. Koelling, M.A. Verheijen, L.P. Kouwenhoven, C.J. Palmstrøm, and E.P.A.M. Bakkers, Nature **548**, 434 (2017).
[20] H. Zhang, C.X. Liu, S. Gazibegovic, D. Xu, J.A. Logan, G. Wang, N. van Loo, J.D.S. Bommer, M.W.A. de Moor, D. Car, R.L.M. Op het Veld, P.J. van Veldhoven, S. Koelling, M.A. Verheijen, M. Pendharkar, D.J. Pennachio, B. Shojaei, J.S. Lee, C.J. Palmstrom, E.P.A.M. Bakkers, S. Das Sarma, and L.P. Kouwenhoven, Nature **556**, 74 (2018).
[21] S. Vaitiekenas, M.T. Deng, P. Krogstrup, and C.M. Marcus, arXiv:1809.05513.
[22] R.S. Deacon, J. Wiedenmann, E. Bocquillon, F. Domínguez, T.M. Klapwijk, P. Leubner, C. Brüne, E.M. Hankiewicz, S. Tarucha, K. Ishibashi, H. Buhmann, and L.W. Molenkamp, Phys. Rev. X **7**, 021011 (2017).
[23] E. Bocquillon, R.S. Deacon, J. Wiedenmann, P. Leubner, T.M. Klapwijk, C. Brüne, K. Ishibashi, H. Buhmann, and L.W. Molenkamp, Nat. Nanotechnol. **12**, 137 (2017).
[24] D. Laroche, D. Bouman, D.J. van Woerkom, A. Proutski, C. Murthy, D.I. Pikulin, C. Nayak, R.J.J. van Gulik, J. Nygård, P. Krogstrup, L.P. Kouwenhoven, and A. Geresdi, arXiv:1712.08459.
[25] A. Fornieri, A.M. Whiticar, F. Setiawan, E.P. Marín, A.C.C. Drachmann, A. Keselman, S. Gronin, C. Thomas, T. Wang, R. Kallaher, G.C. Gardner, E. Berg, M.J. Manfra, A. Stern, C.M. Marcus, and F. Nichele, arXiv:1809.03037.
[26] C. Moore, T.D. Stanescu, and S. Tewari, Phys. Rev. B **97**, 165302 (2018).
[27] A. Vuik, B. Nijholt, A.R. Akhmerov, and M. Wimmer, arXiv:1806.02801.
[28] D. Bagrets and A. Altland, Phys. Rev. Lett. **109**, 227005 (2012).
[29] J. Liu, A.C. Potter, K.T. Law, and P.A. Lee, Phys. Rev. Lett. **109**, 267002 (2012).
[30] H.J. Kwon, K. Sengupta, and V.M. Yakovenko, Eur. Phys. J. B **37**, 349 (2004).
[31] J. Michelsen, V.S. Shumeiko, and G. Wendin, Phys. Rev. B **77**, 184506 (2008).
[32] C.K. Chiu and S. Das Sarma, arXiv:1806.02224.
[33] A. Zazunov, S. Plugge, and R. Egger, Phys. Rev. Lett. (in press); arXiv:1809.06892.
[34] L. Fu, Phys. Rev. Lett. **104**, 056402 (2010).
[35] B. Béri and N.R. Cooper, Phys. Rev. Lett. **109**, 156803 (2012).
[36] A. Altland and R. Egger, Phys. Rev. Lett. **110**, 196401 (2013).
[37] B. Béri, Phys. Rev. Lett. **110**, 216803 (2013).
[38] A. Haim, E. Berg, F. von Oppen, and Y. Oreg, Phys. Rev. Lett. **114**, 166406 (2015).
[39] A. Haim, E. Berg, F. von Oppen, and Y. Oreg, Phys. Rev. B **92**, 245112 (2015).
[40] D.E. Liu, M. Cheng, and R.M. Lutchyn, Phys. Rev. B **91**, 081405 (2015).
[41] K.M. Tripathi, S. Das, and S. Rao, Phys. Rev. Lett. **116**, 166401 (2016).
[42] T. Jonckheere, J. Rech, A. Zazunov, R. Egger, and T. Martin, Phys. Rev. B **95**, 054514 (2017).
[43] A. Zazunov, R. Egger, M. Alvarado, and A.L. Yeyati, Phys. Rev. B **96**, 024516 (2017).
[44] A. Zazunov, A. Iks, M. Alvarado, A.L. Yeyati, and R. Egger, Beilstein J. Nanotechnol. **9**, 1659 (2018).
[45] C.J. Bolech and E. Demler, Phys. Rev. Lett. **98**, 237002 (2007).
[46] J. Nilsson, A.R. Akhmerov, and C.W.J. Beenakker, Phys. Rev. Lett. **101**, 120403 (2008).
[47] A. Golub and B. Horovitz, Phys. Rev. B **83**, 153415 (2011).
[48] B.H. Wu and J.C. Cao, Phys. Rev. B **85**, 085415 (2012).
[49] J. Liu, F.-C. Zhang, and K.T. Law, Phys. Rev. B **88**, 064509 (2013).
[50] D. Giuliano, S. Paganelli, and L. Lepori, Phys. Rev. B **97**, 155113 (2018).
[51] A. Zazunov, R. Egger, and A. Levy Yeyati, Phys. Rev. B **94**, 014502 (2016).
[52] D.M. Badiane, M. Houzet, and J.S. Meyer, Phys. Rev. Lett. **107**, 177002 (2011).
[53] M. Houzet, J.S. Meyer, D.M. Badiane, and L.I. Glazman, Phys. Rev. Lett. **111**, 046401 (2013).
[54] A. Zazunov, R. Egger, C. Mora, and T. Martin, Phys. Rev. B **73**, 214501 (2006).

[55] See the appendix, where we provide additional details on the derivation of Eq. (15), about the effects of MAR processes and of low-lying subgap quasi particles on shot noise, and about other voltage configurations.
[56] A. Martín-Rodero, A. Levy Yeyati, F.J. García-Vidal, Phys. Rev. B **53**, R8891 (1996).
[57] D. Averin and H.T. Imam, Phys. Rev. Lett. **76**, 3814 (1996).
[58] I. S. Gradshteyn and I. M. Ryzhik, *Table of Integrals, Series, and Products* (Academic, Elsevier, New York, 2007).
[59] A. Levy Yeyati, A. Martin-Rodero, and E. Vecino, Phys. Rev. Lett. **91**, 266802 (2003).